Biophysical Characterization of Anticoagulant Hemextin AB Complex from the Venom of Snake *Hemachatus haemachatus*

Yajnavalka Banerjee,*† Rajamani Lakshminarayanan,‡§ Subramanian Vivekanandan,*¶ Ganesh Srinivasan Anand,* Suresh Valiyaveettil,‡ and R. Manjunatha Kini*‖

*Department of Biological Sciences, Faculty of Science, and ‡Department of Chemistry, National University of Singapore, Singapore; †Department of Molecular and Experimental Medicine, The Scripps Research Institute, La Jolla, California; §School of Dentistry, Center for Craniofacial Molecular Biology, University of Southern California, Los Angeles, California; ¶Division of Structural and Computational Biology, School of Biological Sciences, Nanyang Technological University, Singapore; and ‖Department of Biochemistry, VCU Medical Center, Medical College of Virginia, Virginia Commonwealth University, Richmond, Virginia

ABSTRACT Hemextin AB complex from the venom of *Hemachatus haemachatus* is the first known natural anticoagulant that specifically inhibits the enzymatic activity of blood coagulation factor VIIa in the absence of factor Xa. It is also the only known heterotetrameric complex of two three-finger toxins. Individually only hemextin A has mild anticoagulant activity, whereas hemextin B is inactive. However, hemextin B synergistically enhances the anticoagulant activity of hemextin A and their complex exhibits potent anticoagulant activity. In this study we characterized the nature of molecular interactions leading to the complex formation. Circular dichroism studies indicate the stabilization of β-sheet in the complex. Hemextin AB complex has an increased apparent molecular diameter in both gas and liquid phase techniques. The complex formation is enthalpically favorable and entropically unfavorable with a negative change in the heat capacity. Thus, the anticoagulant complex shows less structural flexibility than individual subunits. Both electrostatic and hydrophobic interactions are important for the complexation; the former driving the process and the latter helping in the stabilization of the tetramer. The tetramer dissociates into dimers and monomers with the increase in the ionic strength of the solution and also with increase in the glycerol concentration in the buffer. The two dimers formed under each of these conditions display distinct differences in their apparent molecular diameters and anticoagulant properties. Based on these results, we have proposed a model for this unique anticoagulant complex.

INTRODUCTION

Blood coagulation is a physiological response to vascular injury that results in the formation of hemostatic plug, which prevents blood loss (1,2). The process is initiated by tissue factor (TF), a cellular receptor for the activated coagulation factor VIIa (FVIIa), which is exposed after vascular injury (3). FVIIa bound to TF activates factor X (FX) and factor IX. Activated factor X (FXa) converts small amounts of prothrombin to thrombin (4). Thrombin in turn amplifies the coagulation cascade by activating the platelets (5) and factors (6) and VIII (7,8). Coagulation is propagated when factor IXa binds to factor VIIIa to form intrinsic tenase, a complex that efficiently activates FX. FXa then binds to factor Va to form prothrombinase, thereby increasing the rate of FXa-mediated conversion of prothrombin to thrombin by >300,000-fold (9). The resultant burst of thrombin rapidly converts fibrinogen to fibrin. Fibrin monomers polymerize to form the fibrin mesh that is stabilized and cross-linked by transglutaminase factor XIIIa (10,11). Thus the initial formation of TF-FVIIa complex is crucial for the clot initiation and is considered an ideal target for the treatment of thromboembolic disorders. Drugs that target this complex are potent inhibitors of coagulation and thus are highly sought after. Though, naturally occurring inhibitors of FVIIa have been identified, they are not specific. For example, dysinosin A isolated from the sponge family Dysideidae inhibits FVIIa with a K_i of 108 nM. However, it also an inhibitor of thrombin (12,13). Until recently only two natural anticoagulants targeting specifically the TF-FVIIa complex has been identified. They are tissue factor pathway inhibitor (TFPI) (14,15) and nematode anticoagulant peptide (NAPc2) (16,17). TFPI is a 42-kDa plasma glycoprotein consisting of three tandem Kunitz-type domains. The first and second domains inhibit TF-FVIIa and FXa, respectively. The third Kunitz domain and the C-terminal basic region of the molecule have heparin-binding sites. The anticoagulant action of TFPI is a two-stage process. The second Kunitz domain binds first to a molecule of FXa and deactivates it. The first domain then rapidly binds to an adjacent TF-FVIIa complex, preventing further activation of FX (18–20). On the other hand, NAPc2 is an 8-kDa short polypeptide. It first binds to FXa or zymogen FX to form a binary complex before its interaction and inhibition of membrane-bound TF-FVIIa (21). Therefore, despite the structural differences, both inhibitors form a quaternary complex with TF-FVIIa-FXa. Further, in both the complexes the active site of FVIIa is occupied by the respective inhibitors and is not accessible.

Snake venoms are veritable gold mines of anticoagulant proteins (22,23). Recently, we isolated and characterized a novel anticoagulant protein complex (hemextin AB complex) from the venom of elapid snake *Hemachatus haemachatus* (African ringhals cobra) (24,25). Hemextin AB complex

Submitted October 31, 2006, and accepted for publication July 5, 2007.

Address reprint requests to R. Manjunatha Kini, Protein Science Laboratory, Dept. of Biological Sciences, Faculty of Science, National University of Singapore, Singapore 117 543. E-Mail: dbskinim@nus.edu.sg.

Editor: Marcia Newcomer.

0006-3495/07/12/3963/14 $2.00

doi: 10.1529/biophysj.106.100164

specifically and noncompetitively inhibits the TF-FVIIa complex with a K_i of 25 nM. Further, it inhibits FVIIa in the absence of TF and FX. Thus, unlike TFPI and NAPc2, this unique complex neither requires FX scaffold nor does it bind to the active site of FVIIa (24).

Structurally, hemextin AB complex consists of two proteins—hemextin A and hemextin B, both of which belong to the three-finger toxin family of snake venom proteins. Individually, only hemextin A exhibits a mild anticoagulant activity, whereas hemextin B is inactive. However, hemextin B synergistically enhances the anticoagulant activity of hemextin A and their complex has potent anticoagulant activity. Thus, the formation of this unique synergistic complex of three-finger toxins is important for its ability to inhibit clot initiation (24). There are only a few noncovalent protein complexes in snake venoms that do not contain phospholipase A_2 as an integral part, such as rhodocetin (26,27) and pseutarin C (28,29). Hemextin AB complex is the only known snake venom protein complex formed by the interaction between two three-finger toxins and is the only known heterotetrameric complex of three-finger toxins.

Since hemextin AB complex is both structurally and functionally unique, we have investigated the molecular interactions involved in the formation of this novel complex. In particular we have examined the role of electrostatic and hydrophobic interactions in the formation of tetrameric anticoagulant complex. Hemextin AB complex has identical molecular diameter in both gas and solution phases. Isothermal titration calorimetry (ITC) studies reveal that the complex formation is entropically unfavored, which indicates the reduced structural flexibility of the complex. Hemextin AB assembly is an enthalpically driven process with some conformational changes accompanying the complexation. The tetrameric complex behaves differently in buffers of higher ionic strength. It is also sensitive to the presence of glycerol in the buffer solution. Thus, a complex interplay of electrostatic and hydrophobic interactions drives the formation and stabilization of this novel anticoagulant protein complex. Based on our observations, we propose a model for the assembly of hemextin AB complex.

MATERIALS AND METHODS

Purification of hemextins A and B

Hemextin A and hemextin B were purified using the methods described earlier (24). Briefly, *H. haemachatus* crude venom (100 mg in 1 ml distilled water) was applied to a Superdex 30 gel filtration column (1.6 × 60 cm) equilibrated with 50 mM Tris-HCl buffer (pH 7.4) and eluted using the same buffer, using an ÄKTA Purifier system (Amersham Biosciences, Uppsala, Sweden). Fractions containing potent anticoagulant activity were pooled and subfractionated on a Uno S-6 (Bio-Rad, Hercules, CA; column volume, 6 ml) cation-exchange column. The peaks containing hemextin A and hemextin B were further purified using reversed-phase high-performance liquid chromatography (RP-HPLC) on a Jupiter C18 (1 × 25 cm) column. Both proteins were found to be homogeneous with molecular masses of 6835.00 ± 0.52 and 6792.56 ± 0.32 Da, respectively, as determined by electrospray ionization mass spectrometry (ESI-MS) (24).

Circular dichroism spectroscopic studies

Far-ultraviolet (UV) circular dichroism (CD) spectra (260–190 nm) were recorded using a Jasco J-810 spectropolarimeter (Jasco, Tokyo, Japan). All measurements were carried out at room temperature (25°C) using 0.1 cm pathlength stoppered cuvettes. The instrument optics was flushed with 30 l/min of nitrogen gas. The spectra were recorded using a scan speed of 50 nm/min, resolution 0.2 nm, and bandwidth 2 nm. For each spectrum, a total of six scans were recorded, averaged, and baseline subtracted. The conformation of hemextin A and hemextin B at different concentrations were monitored in 50 mM Tris-HCl buffer (pH 7.4). To study the complex formation, titration experiments were carried out by keeping the concentration of hemextin A constant at 0.5 mM, and varying the concentration of hemextin B.

Determination of molecular diameters

The apparent molecular diameters of the hemextin AB complex and the individual hemextins were determined in both the gas and solution phases using Gas Phase Electrophoretic Mobility Macromolecule Analyzer (GEMMA) and dynamic light scattering (DLS), respectively.

GEMMA

The molecular diameters in the gas phase were determined with GEMMA (30) using a nano-differential mobility analyzer, model 3980, with a standard condensation particle counter, type 3025 (TSI, St Paul, MN). The instrument was operated in the ''cone jet'' mode with an operating voltage between 2.5 and 3.0 kV, resulting in currents from 200 to 300 nA. Filtered ambient air at 2 l/min and a concentric sheath gas flow of filtered CO_2 at 0.1 l/min was used to stabilize the electrospray against corona discharge. Sample solutions of hemextin A (4 ng/ml) and hemextin B (4 ng/ml) were prepared in 20 mM ammonium acetate (pH 7.4) immediately before the experiment. Hemextin AB complex (4.5 ng/ml) was reconstituted in the above buffer and was incubated at 37°C for 10 min. Another three-finger protein, toxin C, isolated and purified from the same venom, was used as a control in the GEMMA experiments. The samples were infused into the electrospray chamber with an inlet flow rate of 100 nl/min. Twenty scans over the whole electrophoretic mobility (EM) diameter range (0–25 nm) were recorded and averaged to obtain a GEMMA spectrum. Data presentation was done without the application of any smoothing algorithm.

DLS

The complex formation studies with DLS were carried out at 25°C using a BI200SM instrument (Brookhaven Instruments, Holstville, NY). A vertically polarized argon ion laser (514.2 nm, 75 mW; NEC model GLG-3112) was used as the light source. Sample solutions of hemextin A (4 mM), hemextin B (4.1 mM), and hemextin AB complex (4.6 mM) in 50 mM Tris-HCl buffer (pH 7.4) were prepared immediately before the experiment. The hydrodynamic diameter for the hemextin AB complex and the individual hemextins were recorded at 25°C in solutions of different ionic strengths and at different glycerol concentrations. The ionic strengths were varied by the addition of NaCl. From the measured translational diffusion coefficient (D_T), the hydrodynamic radius (R_H) can be calculated using the Stokes-Einstein relation:

$$D_T = k_B T / 6\pi\eta R_H, \quad (1)$$

where, k_B is the Boltzmann constant, T is the temperature in Kelvin, and η is the viscosity of the solvent. The intensity-intensity time correlation functions were obtained with a BI-9000 digital correlator. The particle size and size distribution were obtained by analyzing the field correlation function $|g^{(1)}(\tau)|$ using constrained regularized CONTIN method (31).

Thermodynamics of hemextin AB complex formation

ITC experiments were performed using a Microcal VP-ITC calorimeter (Microcal LLC, Northampton, MA) to study the thermodynamics of the formation of hemextin AB complex. Unless otherwise noted, all experiments were performed in 50 mM Tris-HCl buffer (pH 7.4). Both the proteins were dissolved in the same buffers, filtered and degassed before titration. Hemextin A (0.1 mM) was kept in the sample cell and hemextin B (1 mM) was loaded into the syringe. The syringe stirring speed was set to 300 rpm. Data were collected in high feedback mode, with a filter period of 3 s. For each experiment, a control titration was performed by injecting hemextin B into the appropriate buffer. Finally, the control data were subtracted from the raw data to obtain an isotherm corrected for heats of dilution. The first injections presented defects in the baseline and these data points were not included in the fitting process. The calorimetric data were processed and fitted to the single set of identical sites model using Microcal Origin (Version 7.0) data analysis software supplied with the instrument. The expression for the heat released per injection, $\Delta Q_{(i)}$, is given by

$$\Delta Q_{(i)} = Q_{(i)} + dV_i / 2V_0[Q(i) + Q(i-1)] - Q(i-1), \quad (2)$$

where $Q_{(i)}$ is the total heat content, dV_i is the volume injected at the ith injection, and V_0 is the cell volume. The total heat content Q of the solution (determined relative to zero for the unliganded species) contained in the active cell volume, V_0, was calculated according to Eq. 3, where K_A is the binding affinity constant, n is the number of sites, ΔH is the enthalpy of ligand binding, and M_t and X_t are the bulk concentration of macromolecule and ligand, respectively, for the binding $X + M \leftrightarrow XM$

$$Q = \frac{nM_t\Delta HV_0}{2}\left[1 + \frac{X_t}{nM_t} + \frac{1}{nK_aM_t} - \sqrt{\left(1 + \frac{X_t}{nM_t} + \frac{1}{nK_aM_t}\right)^2 - \frac{4X_t}{nM_t}}\right]. \quad (3)$$

The change in heat (ΔQ) measured between the completions of two consecutive injections is corrected for dilution of the protein and ligand in the cell according to standard Marquardt method (32,33). The free energy change (ΔG) during the interaction was calculated using the relationship: ($\Delta G = \Delta H - T\Delta S = -RT\ ln\ K_a$). All the experiments were performed at 37°C unless otherwise indicated.

The role of electrostatic interactions in the complex formation was evaluated by performing ITC experiments in 50 mM Tris-HCl buffer of various ionic strengths. The ionic strengths of the buffers were altered by adding sodium chloride (NaCl) (35–150 mM). To study the role of hydrophobic interactions in the complex formation, experiments were performed in 50 mM Tris-HCl buffer (pH 7.4) containing various concentrations of glycerol (125–250 mM).

Size-exclusion chromatography studies

All size-exclusion chromatography (SEC) experiments were carried out at room temperature on a prepacked Superdex 75 gel filtration column (1.6 × 60 cm) using a ÄKTA Purifier system (Amersham Biosciences, Uppsala, Sweden). The column was eluted with 50 mM Tris-HCl buffer (pH 7.4) or the specified elution buffer, at a flow rate of 1 ml/min. The sample volume applied to the column was 4 ml. The column was calibrated using ovomucoid (28 kDa) ribonuclease (15.6 kDa), cytochrome C (12 kDa), apoprotinin (7 kDa), and pelovaterin (4 kDa) (34) as molecular weight markers. The void volume was determined by running Blue Dextran. The column was equilibrated with at least two bed volumes of the elution buffer before each run. Electrostatic contributions in the hemextin AB complex formation were studied by monitoring its elution in 50 mM Tris-HCl buffer (pH 7.4) with different concentrations of NaCl (75 and 150 mM). Hydrophobic contributions for the complex formation were determined by recording the elution of hemextin AB complex in 50 mM Tris-HCl buffer (pH 7.4) with different concentrations of glycerol (125 and 250 mM). In both the studies, the column was first equilibrated with the desired buffer before the application of the reconstituted hemextin AB complex in the respective buffer to the column. The protein elution was monitored by recording absorbance at 280 nm.

Anticoagulant activity

The anticoagulant activity of individual hemextins and hemextin AB complex were determined using prothrombin time clotting assay (A. J. Quick, 1935). The anticoagulant activity of a specific concentration of hemextin A (4.4 μM), hemextin B (4.4 μM), and hemextin AB complex (0.22 μM) was monitored in 50 mM Tris-HCl (pH 7.4) containing different concentrations of NaCl (35–150 mM for studying the role of electrostatic interactions) and glycerol (125–250 mM for studying the role of hydrophobic interactions). The concentrations of hemextin A and hemextin AB complex were chosen in a way such that in the absence of salt/glycerol the recorded clotting times are similar. Control experiments were performed without the addition of the anticoagulant proteins to evaluate the effect of salt and glycerol on clotting.

One-dimensional NMR spectroscopy

One-dimensional (1D) proton NMR experiments were carried out using Bruker 700 MHz spectrometer (Billerica, MA), equipped with a modern cryoprobe, and electronic variable temperature unit. The spectra were acquired using Topspin software (Bruker) interfaced to the spectrometer. Hemextin A (0.5 mM) and hemextin B (0.5 mM) were prepared in 50 mM Tris-HCl buffer (pH 7) and transferred to a 5-mm diameter Willmad NMR tube. All deuterated solvents were purchased from Aldrich Laboratories (Milwaukee, WI) with 99.9% isotopic purity. The spectral width was set to 11,202 Hz for all NMR experiments. The huge resonance due to the water protons was suppressed by the WATERGATE pulse sequence (35). Typically, 512 scans were averaged for each free induction decay before apodization and then performing the Fourier transformation. ^{1}H chemical shifts were referenced to a sodium 2,2-dimethyl-2-silapentane-5-sulfonate solution (DSS).

RESULTS AND DISCUSSION

Conformational changes during the complex formation

It has been shown previously that hemextin A and hemextin B interact with each other and form a 1:1 heterotetrameric complex and this complex formation is important for its ability to inhibit FVIIa and clot initiation (24). To study the conformational changes associated with the hemextin AB complex formation we used far-UV CD. First, we recorded the CD spectra of individual hemextins A and B (Fig. 1, *A* and *B*). Their CD spectra display negative minima at 217 nm and positive maxima at 196 nm, which are due to the n to π^* transition and the π to π^* transition of the amide chromophore, respectively, typical of a β-sheet structure (Fig. 1, *A* and *B*). Next, a titration CD experiment was performed to study the complex formation between the two proteins. In this experiment, the concentration of hemextin A was kept constant at 0.5 mM and the conformational changes in hemextin A in the presence of various concentrations of hemextin B were recorded. The shape of the CD spectrum upon addition of hemextin B to hemextin A did not change significantly

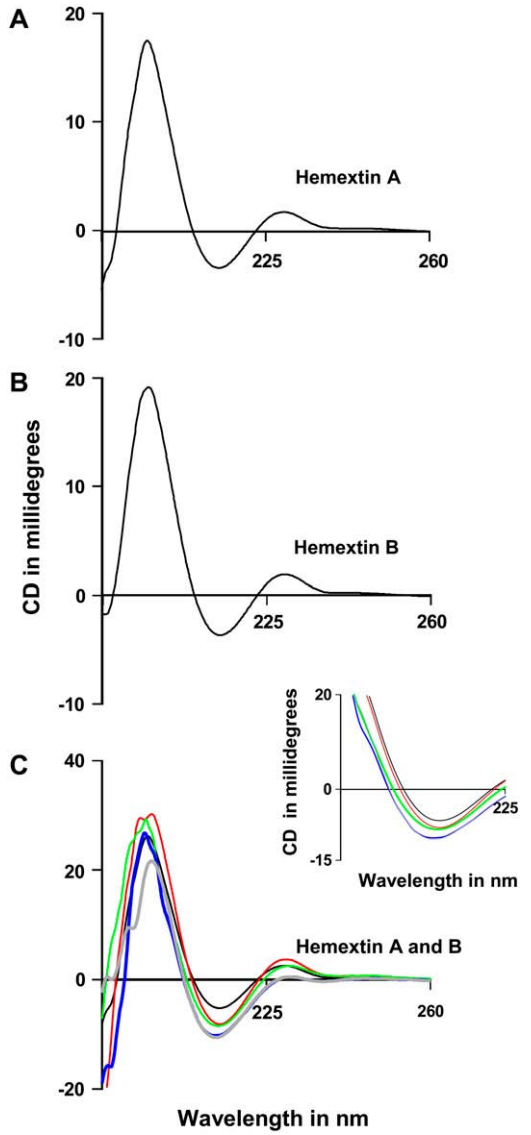

FIGURE 1 Conformational changes associated with the formation of hemextin complex. CD spectra of (*A*) hemextin A (0.5 mM) and (*B*) hemextin B (0.5 mM). (*C*) Conformational changes in hemextin A with increasing concentrations of hemextin B: (*black*) hemextin A 0.5 mM; (*red*) hemextin A 0.5 mM plus hemextin B 0.25 mM; (*green*) hemextin A 0.5 mM plus hemextin B 0.4 mM; (*blue*) hemextin A 0.5 mM plus hemextin B 0.5 mM; (*gray*) hemextin A 0.5 mM plus hemextin B 0.9 mM; (*inset*) the observed change in the CD spectra around the 217-nm region.

(Fig. 1 *C*). However, the CD intensity at 217 nm increases with the incremental addition of hemextin B and reaches maximum at the 1:1 molar ratio suggesting increase in β-sheet content and stoichiometric binding of hemextin B to hemextin A, respectively (see Supplementary Material, Fig. S1A). The difference spectrum obtained by subtracting the CD spectrum of 1:1 complex from the sum of the CD spectra of hemextin A and hemextin B indicates the conservation of β-sheet structure in the complex, suggesting possible folding upon complex formation. (see Supplementary Material, Fig. S1B).

Changes in molecular diameters during the complex formation

The diameter of the individual hemextins and hemextin AB complex were determined in both gas and solution phases. In the gas phase analyses using GEMMA, hemextin A, and hemextin B showed the apparent molecular diameters of 10.20 $\pm$ 0.38 nm and 8.82 $\pm$ 0.42 nm, respectively (Fig. 2). Hemextin AB complex exhibited a larger diameter of 16.30 $\pm$ 0.43 nm. To further confirm on the GEMMA results, we examined the effect of toxin C, another three-finger toxin isolated from the venom of *H. haemachatus*, on the molecular diameters of hemextins A and B, to determine the specificity of interaction. Toxin C did not affect the anticoagulant activity of hemextin A in prothrombin time clotting assay (data not shown) and did not form a complex with hemextin A. At equimolar concentration of toxin C, the molecular diameter of hemextin A or hemextin B remains unaffected (Fig. 2). The solution phase studies with DLS also confirmed the increase in molecular diameter associated with the complex formation. Single scattering populations (unimodal distribution) for hemextin A, hemextin B, and hemextin AB complex were

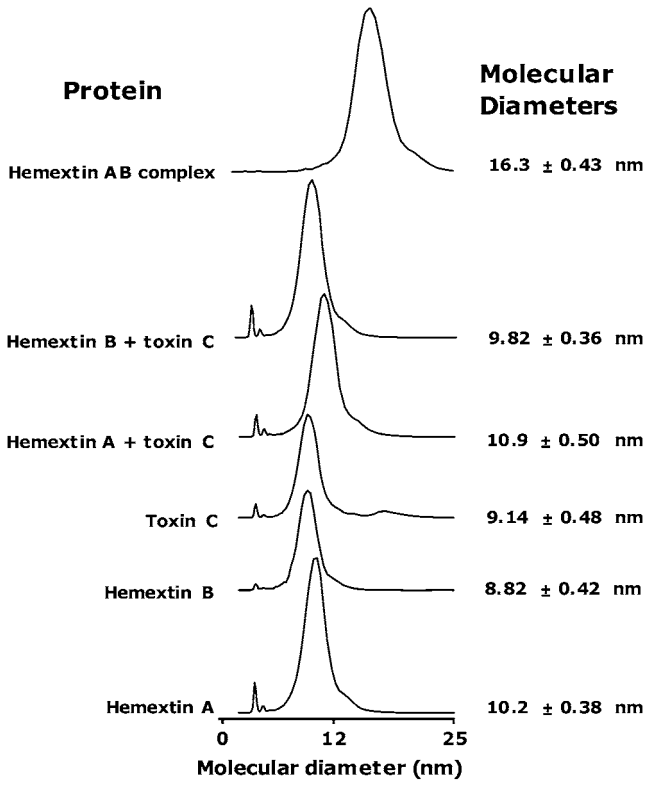

FIGURE 2 Measurement of molecular diameter during the hemextin AB complex formation using GEMMA. The molecular diameters of the individual hemextins and the hemextin AB complex are calculated based on their electrophoretic mobility. The formation of hemextin AB complex leads to an increase in the molecular diameter. Addition of equimolar toxin C does not show any significant increase in the molecular diameters of hemextin A and hemextin B validating the obtained data.

observed in DLS suggesting the homogeneity of the sample preparations with hydrodynamic diameters of 10.3, 9.9, and 16.8 nm, respectively (Fig. 3 *A*). The narrow size distribution of a single monodisperse species for 1:1 mixture of hemextin A and hemextin B suggests the formation of a well-defined complex. It is important to note that the tetrameric hemextin AB complex and individual hemextins exhibited comparable molecular diameters in both gas and solution phases. The apparent molecular dimensions are significantly larger than the theoretical diameter estimated for a native protein and much smaller than the estimated length of the proteins in completely ''extended conformation'' (36,37). Such an anomaly could be due to the nonglobular conformation of the proteins (38). The molecular diameter of hemextin AB complex is, however, much smaller compared to the estimated size of a tetramer indicating that the four monomers are compactly packed.

Thermodynamics of the hemextin AB complex formation

ITC permits the study of macromolecular interactions in solution and is the only technique that can resolve the enthalpic and entropic components of binding affinity (39–41). It was used to study the thermodynamics of hemextin AB complex formation. Each injection gave rise to negative (exothermic) heat of reaction (Fig. 4). The binding isotherm fits to a single set of binding sites model, suggesting an equimolar binding between hemextin A and hemextin B. The interaction between them is thermodynamically allowed (as indicated by negative ΔG) (Table 1). A favorable negative ΔH but unfavorable negative ΔS changes indicate that the complex formation is enthalpically driven, and van der Waals interactions and hydrogen bonds may play an important role in the complex formation (42). Also, the formation of a less dynamic complex is entropically disfavored, as has been observed in the studies pertaining to the dimerization of insulin (43). Thus the recorded negative entropic change (ΔS) indicates the formation of a less flexible or less disordered hemextin AB complex. The binding constant (K_A) for the formation of hemextin AB complex was $2.23 \times 10^6\ M^{-1}$ and it falls within the K_A values for protein-protein interactions in biologically relevant processes that range from 10^4 to $10^{16}\ M^{-1}$ (44).

The effect of temperature on the hemextin AB complex formation

To further understand energetics of the complex formation, complete temperature profile of the thermodynamic parameters associated with the binding of hemextin A to hemextin B was studied over the temperature range of 25–45°C. The temperature dependence of ΔH is shown in Fig. 5 *A* and Table 1. The temperature dependence of ΔH over a narrow temperature range is given by the equation:

$$\Delta H = \Delta H_0 + \Delta C_p(T - T_0), \quad (4)$$

where, ΔH_0 is the binding enthalpy at an arbitrary reference temperature and ΔC_p is the heat capacity change of binding. The ΔC_p obtained from the slope ($\Delta C_p = \delta\Delta H / \delta T$) (Fig. 5 *A*) is -163 cal/K^{-1}mol^{-1}. Negative ΔCp indicates a reduction in the nonpolar solvent-accessible surface area, as explained by the following equation (45,46),

$$\Delta C_p = 0.45(\Delta ASA_{nonpol}) - 0.26(\Delta ASA_{pol})\ \text{cal/molK}, \quad (5)$$

where, ΔASA_{pol} and ΔASA_{nonpol} are the change in the polar- and nonpolar-accessible surface areas, respectively. Thus, hemextin AB complex formation is associated with the burial of hydrophobic surface area.

Fig. 5 *B* shows the plot of ΔG and ΔH as a function of $T\Delta S$. It is clear that the ΔG of binding remained temperature independent and is a result of linear dependence of ΔH on $T\Delta S$. This strongly suggests the enthalpy-entropy compensation for the binding of hemextin A to hemextin B. This phenomenon is a universal feature for protein-peptide interactions, where weak molecular interactions undergo constant rearrangements to realize a lower free energy of binding (42,47–49). The correlation between entropy and enthalpy for a range of interacting protein-protein systems was determined ($r^2 = 0.956$). The data for hemextin AB complex fall well along this correlation line (see Supplementary Material, Fig. S2).

The negative ΔC_p indicates the net thermodynamic driving force for the association to shift from entropic to enthaplic with increasing temperature. At the intersection point of both lines $\Delta G = \Delta H = -8.4$ kcal mol^{-1} (Fig. 5 *B*), which corresponds to a temperature T_s (temperature at which the contribution from entropy is zero (50,51)). At T_s the contribution from entropy changes from favorable to unfavorable. From Fig. 5 *A*, $\Delta H = -8.4$ kcal mol^{-1} is connected with a T_s of 16°C (289 °K).

The negative ΔC_p for the hemextin AB complex formation further suggests that the observed entropy change upon binding must include significant contribution from the hydrophobic effect in the physiological temperature range. Therefore, for protein-protein/ligand interaction(s) the net entropy of association is given by the equation:

$$\Delta S_{assoc} = \Delta S_{HE} + \Delta S_{rt} + \Delta S_{other}, \quad (6)$$

where, ΔS_{HE}, ΔS_{rt}, and ΔS_{other} are the entropy changes due to hydrophobic effect, reduction of rotational and translational degree of freedom, and from other sources, respectively.

At T_s, the overall entropy of association is zero and the above equation becomes:

$$\Delta S_{assoc} = \Delta S_{HE}(T_s) + \Delta S_{rt} + \Delta S_{other} = 0. \quad (7)$$

In the absence of crystallographic data, the $\Delta S_{HE}(T_s)$ was estimated from the equation,

$$\Delta S_{HE}(T_s) = 1.35\Delta C_p \ln(T_s/386), \quad (8)$$

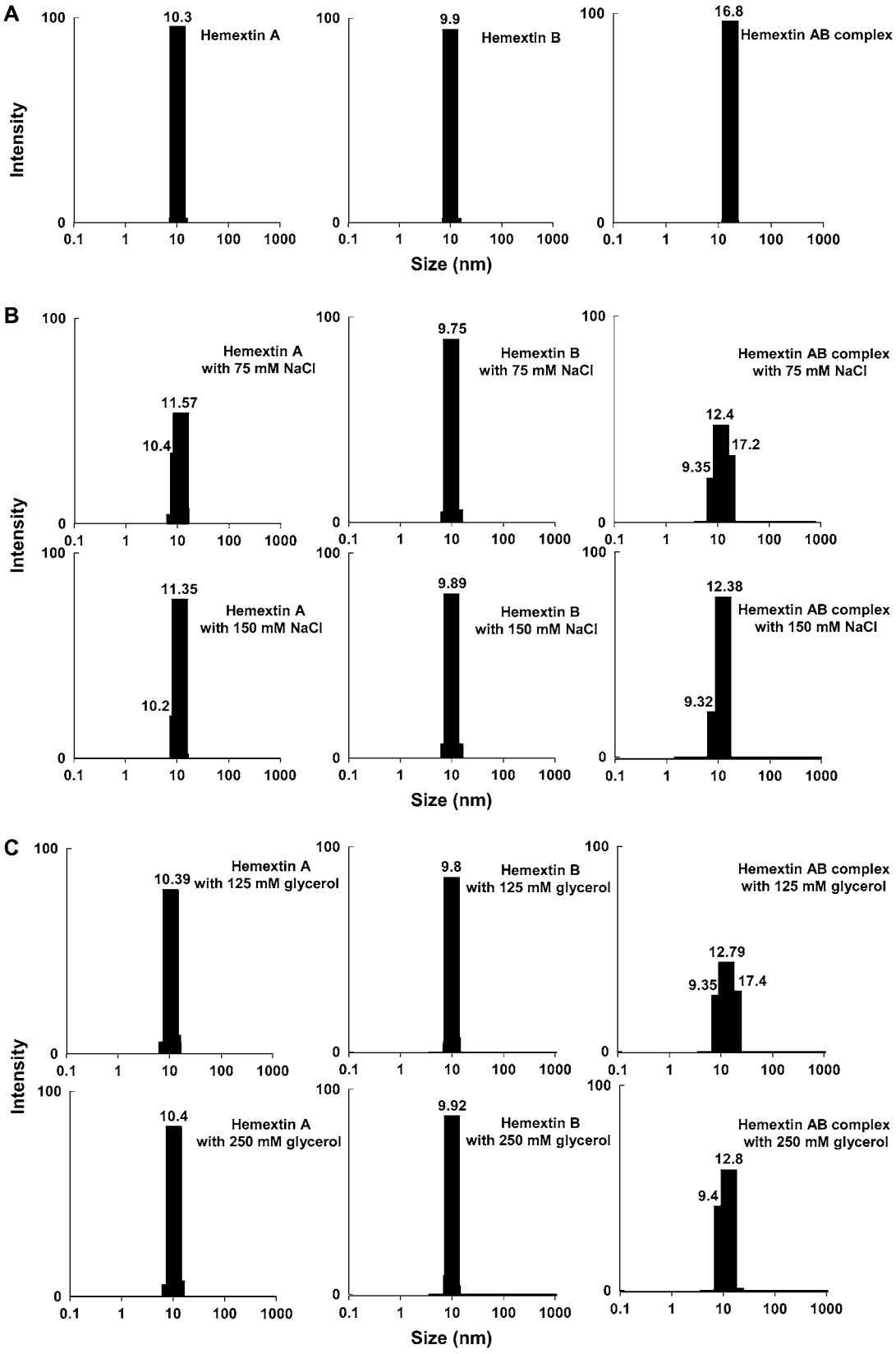

FIGURE 3 Determination of hydrodynamic diameter using DLS. (*A*) CONTIN analysis hemextin A, hemextin B, and hemextin AB complex in 50 mM Tris-HCl buffer. Effect of various concentrations of NaCl (*B*) and glycerol (*C*) on hemextin AB complex. The calculated hydrodynamic diameters for each molecular species are shown. (Note the dimer formed in glycerol has a different diameter than the one formed in salt.)

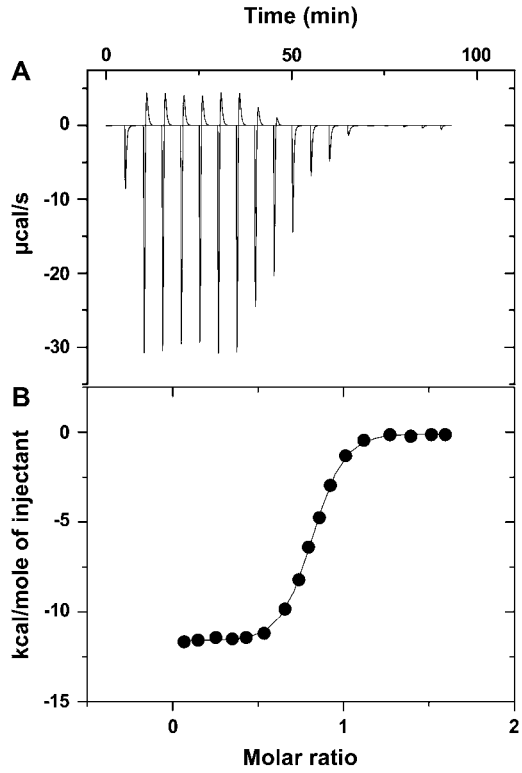

FIGURE 4 Interaction studies between hemextin A and B using ITC. (*A*) Raw ITC data showing heat release upon injections of 1 M hemextin B into a 1.4-ml cell containing 0.1 mM of hemextin A; (*B*) integration of the raw ITC data yields the heat/mol versus molar ratio. The best values of the fitting parameters are 1.04 for N, 2.23×10^6 M^{-1} for K_A, and -11.68 kcal M^{-1} for ΔH (Table 1).

and found to be 64 cal deg^{-1} mol^{-1}. It has been shown that protein-protein interaction ΔS_{rt} is nearly equal to -50 cal deg^{-1} mol^{-1} (52,53). Thus the ΔS_{other} is calculated to be -14 cal deg^{-1} mol^{-1}. Because of experimental uncertainties in the heat capacity change and the entropy of complex formation, as well as in the value of the rotational-translational entropy term, the analysis of coupled folding is typically not suitable for distinguishing small extents of folding from the rigid body case. However, from the nonzero value of ΔS_{other} it can be concluded that that there is no evidence for large-scale coupled folding, during the formation of hemextin AB complex. Again, $\Psi = \Delta S_{other} / -5.6$ cal deg^{-1} mol^{-1}, where Ψ designates the number amino acid residues involved in the folding transition (54). Therefore, approximately three residues are involved in the folding transition. Also, from Fig. 5 *B* the enthalpic counterpart of T_S, namely T_H, the temperature at which the enthalpic contribution to the Gibbs free energy of binding changes from favorable to unfavorable is calculated to be 244 °K. Therefore, below -29°C the binding process is entropically driven and only in the interval between T_S and T_H (i.e., between -29°C and 16°C), both the entropic and enthalpic parts of the Gibbs free energy of binding are favorable.

Oligomerization states of the anticoagulant complex and individual hemextins

Hemextin AB complex exists as a tetramer and the complex formation is pivotal for its potent anticoagulant activity. In addition, as determined in prothrombin time and kinetic assays the stoichiometry of complex formation is 1:1 (24,25). We evaluated the role of both electrostatic and hydrophobic interactions in complex formation.

Electrostatic interactions in hemextin AB complex formation

Firstly, the binding constant for hemextin AB complex formation was determined by ITC in buffers of increasing ionic strength. The log K_A values for the complex formation decreased linearly with the increasing NaCl concentration (Fig. 6 *A*, Table 1), illustrating the participation of electrostatic interactions in complex formation. Secondly, the effect of buffer ionic strength on the assembly of hemextin AB

TABLE 1 Thermodynamic analysis of hemextin A-hemextin B interaction

ITC experiments	$K_A \times 10^6$ (M^{-1})	ΔH (kcal/mol)	ΔS (cal/deg mol)	ΔG (kcal/mol)
At different temperatures (°C)				
25	2.07	−9.92	−4.43	−8.6
37	2.23	−11.7	−8.645	−9
45	1.97	−13.12	−12.49	−9.15
At different salt concentrations				
35 mM NaCl	0.63	−10.5	−7.2	−8.2
75 mM NaCl	0.33	−9.32	−4.8	−7.8
100 mM NaCl	0.02	−7.31	−3.82	−6.12
150 mM NaCl	0.002	−5.01	−1.2	−4.6
At different glycerol concentrations				
125 mM Glycerol	0.32	−10.8	−11.01	−7.6
175 mM Glycerol	0.2	−10.5	−10.6	−7.2
250 mM Glycerol	0.05	−9.4	−10	−6.4

All ITC experiments in salt and glycerol were carried out at 37°C.

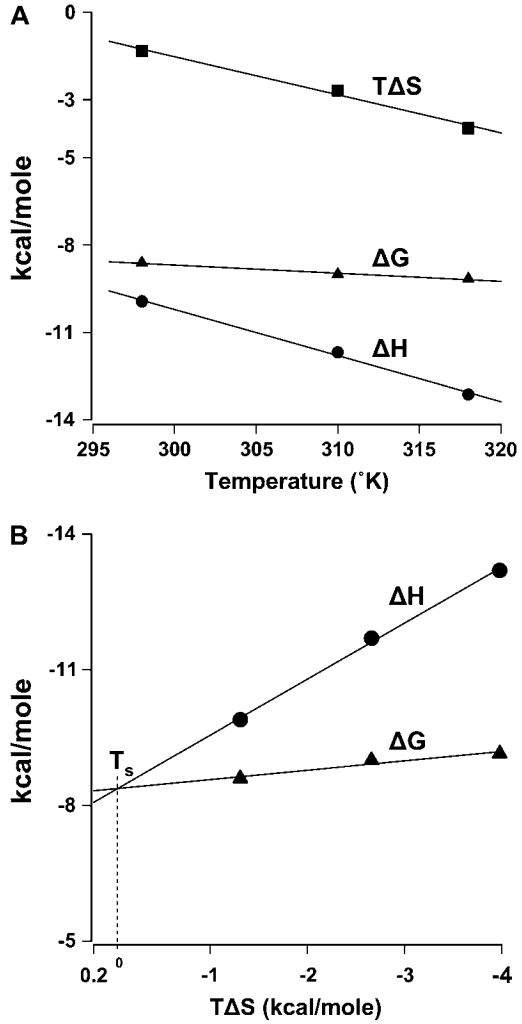

FIGURE 5 Thermodynamics of hemextin A-hemextin B interaction. (*A*) Effect of temperature on the energetics of hemextin A-hemextin B interaction: enthalpy change (ΔH), change in entropy term ($T\Delta S$), and free energy change (ΔG). (*B*) Enthalpy-entropy compensation in complex formation. (Point of intersection of lines corresponding to ΔH and ΔG corresponds to T_s)

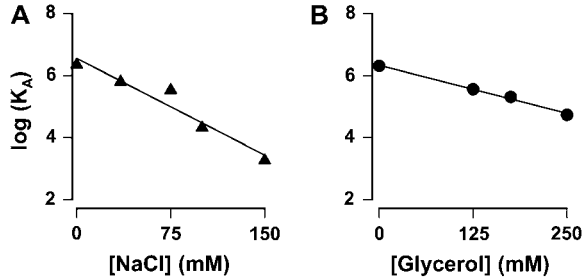

FIGURE 6 Hemextin AB complex formation under different buffer conditions. (*A*) Dependence of K_A on the ionic strength of the buffer. The binding affinity decreases with the increase in buffer ionic strength indicating the importance of electrostatic interactions. (*B*) Dependence of K_A on the glycerol concentration. The binding affinity decreases with the increase in glycerol concentration indicating the importance of hydrophobic interactions.

complex was examined with the help of SEC. In the absence of salt, the complex eluted as a tetramer and the individual hemextins as monomers (Fig. 7 *A*). In the presence of 75 mM NaCl the tetramer started dissociating into dimer (Fig. 7 *B*). With further increase in ionic strength of the buffer (NaCl 150 mM) the complex eluted mostly as a dimer and monomer(s). ESI-MS and HPLC analyses of the dimer peak indicated that it contains both hemextins A and B (data not shown). This observation again reconfirms the importance of electrostatic interactions in hemextin AB assembly. Interestingly, an additional protein peak eluted slower than the monomers indicating hemextin A and/or hemextin B was undergoing a conformational change in buffers of high ionic strength. Therefore, we monitored the elution profiles of individual hemextins in buffers of high ionic strength. Hemextin A at 75 mM NaCl concentration showed two peaks; a second protein peak eluted slower than the monomer (Fig. 7 *B*). With further increase in the ionic strength (NaCl 150 mM) hemextin A eluted mostly in the second peak. ESI-MS and HPLC analyses of this second peak show that it is structurally intact hemextin A (data not shown). Thus, the change in the elution profile of hemextin A in buffers of higher ionic strength hinted a conformational change in the protein, which was further confirmed by 1D NMR studies (see below). Increased ionic strength of buffer did not have any effect on the elution of hemextin B (Fig. 7, *A* and *B*).

We also determined the hydrodynamic diameters of hemextin AB complex and individual hemextins in buffer solutions of high ionic strength using DLS (Fig. 3 *B*). (As GEMMA works on the principle of nano-ESI, we did not determine the molecular diameters in buffers containing high salt using this technique.). At high salt concentrations, the hemextin AB complex exhibits a high polydispersity indicating the presence of different species. At 75 mM NaCl, there are three different populations. In addition to the monomer(s) and the tetramer, there is an additional population with an apparent molecular diameter of 12.4 nm. Based on our SEC results (Fig. 7 *B*), we suggest that the 12.4-nm species could be the dimeric hemextin AB complex. As expected, the population of 12.4-nm species increases when the concentration of NaCl is increased to 150 mM (Fig. 3 *B*). Thus DLS data also suggest the dissociation of the tetrameric complex to a dimer. As expected, polydispersity was also observed with hemextin A in buffers of high ionic strength (Fig. 3 *B*). An additional population of 11.57-nm-sized particle, in addition to its native size of 10.4 nm is observed. Based on the SEC (Fig. 7 *B*) and 1D-NMR (see below), we suggest that the 11.57-nm species represents the conformationally altered form of hemextin A. No change in the hydrodynamic diameter of hemextin B was observed with the increase in buffer ionic strength (Fig. 3 *B*).

To understand the implications of the change in conformation of hemextin A and the breakdown of tetrameric complex, we monitored the anticoagulant activity of the complex and individual hemextins in buffers of high ionic strengths. Higher

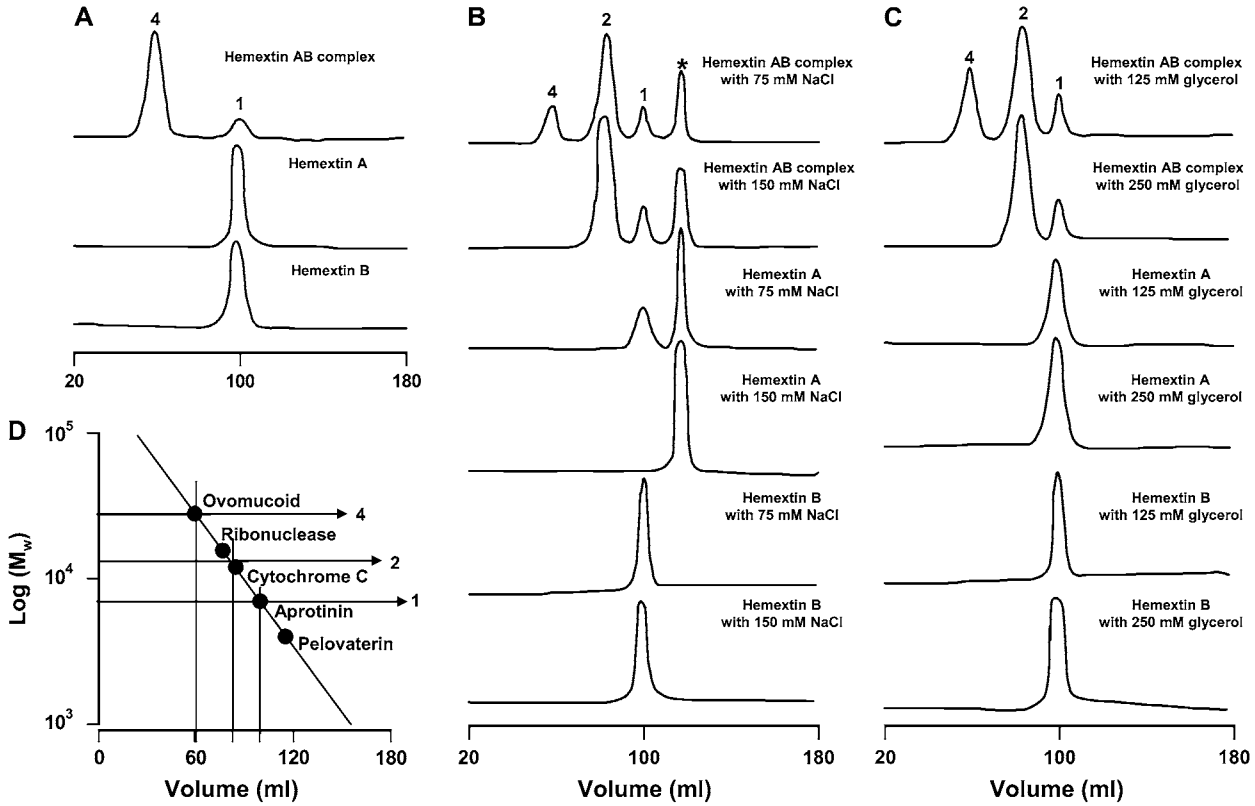

FIGURE 7 SEC studies of hemextin AB complex in different buffer conditions. (*A*) Elution profiles of hemextin AB complex in Tris-HCl buffer. Effect of various concentrations of NaCl (*B*) and glycerol (*C*) on hemextin AB complex. The tetrameric complex (peak denoted by *4*) dissociates into dimer and monomer (peaks denoted by *2* and *1*, respectively) with the increase in salt or glycerol. Asterisk denotes the peak containing conformationally altered hemextin A. (*D*) Calibration of the column using the following proteins as molecular weight markers: ovomucoid (28 kDa), ribonuclease (15.6 kDa), cytochrome C (12 kDa), apoprotinin (7 kDa), and pelovaterin (4 kDa). The molecular weights of the tetramer, dimer, and monomers were calculated from the calibration curve.

concentration of NaCl did not affect the anticoagulant activity of hemextin A (Fig. 8 *A*). Thus despite the change(s) in conformation (see below), hemextin A retains its anticoagulant activity. The anticoagulant activity of hemextin AB complex, in contrast, decreased with the increase in ionic strength up to 100 mM NaCl (Fig. 8 *A*). However, further increase in the salt concentration did not significantly affect the anticoagulant activity. At 150 mM NaCl the complex exists as a mixture of a dimer, monomer(s), and conformationally altered hemextin A as is evident from the SEC experiments (Fig. 7 *B*). Therefore, the remaining anticoagulant activity observed at 150 mM or higher NaCl concentration is due to the presence of monomeric hemextin A and not due to dimeric hemextin AB complex. Hence, it can be concluded that the dimer formed at high salt concentrations does not have any significant anticoagulant activity.

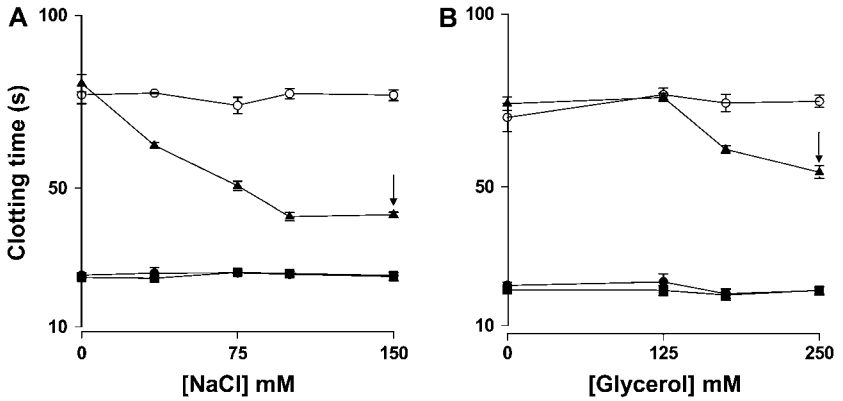

FIGURE 8 Effect of buffer conditions on anticoagulant activity. Effect of various concentrations of NaCl (*A*) and glycerol (*B*) on the anticoagulant activity of hemextin A (O), hemextin B (M), hemextin AB complex (▲). The anticoagulant activity of hemextin AB complex decreases with the increase in concentrations of NaCl and glycerol. The arrows indicate the concentrations of (*A*) NaCl and (*B*) glycerol where the anticoagulant complex exists mostly as a mixture of dimer and monomers (see text for details); (■) denotes the anticoagulant activity recorded in the absence of the proteins.

Thus, these studies in buffers of high ionic strength strongly suggest that electrostatic interactions play crucial role in the assembly of hemextin AB complex. As hemextin A undergoes conformational change(s) in the presence of salt (see below), the dissociation of tetramer in a buffer of high ionic strength may not only be due to the disruption electrostatic interaction but also due to conformational change(s) in hemextin A. Further, high salt concentration leads to the formation of a dimer that is functionally inert (in terms of lack of synergic increase in anticoagulant activity). Based on the obtained results, we hypothesize that the dimer assembled at 150 mM NaCl concentration is probably formed by the interplay of predominantly hydrophobic interactions. Therefore, successive experiments were carried out to evaluate the importance of hydrophobic interactions in the complex formation.

Hydrophobic interactions in the hemextin AB complex formation

We carried out ITC experiments in buffers containing increasing concentrations of glycerol. Adsorption of glycerol to hydrophobic patches on the surface of proteins interferes in the hydrophobic interactions (55,56). A decrease in the association constant was observed with the increase in glycerol concentration (Fig. 6 *B* and Table 1), showing the importance of hydrophobic interactions in the complex formation. We monitored the elution of hemextin AB complex in buffers containing glycerol on a Superdex 75 column (Fig. 7 *C*). In buffers containing high glycerol concentration the tetramer dissociates into dimer and monomers. ESI-MS and HPLC analyses of the dimer peak indicate that it contains both hemextins A and B (data not shown). However, no additional peak corresponding to altered conformation of hemextin A was observed. The elution of individual hemextins remained unaltered in the presence of glycerol (Fig. 7 *C*). The breakdown of hemextin AB complex in the presence of glycerol was also observed in the DLS studies (Fig. 3 *C*). At 125 mM glycerol concentration, an additional population of 12.8-nm-sized species was observed in addition to the monomers and the tetrameric complex. Based on SEC studies, we propose that the 12.8-nm species is a dimer. The 12.8-nm species increases with the increase in glycerol concentration (Fig. 3 *C*). It is important to note that the apparent molecular diameter of this dimer is different from the dimer formed in buffers of high ionic strength (12.8 vs. 12.4 nm; Fig. 3, *B* and *C*). (As GEMMA works on the principle of nano-ESI, we did not determine the molecular diameters in buffers containing glycerol using this technique.). No polydispersity was observed in the case of individual hemextins in the presence of glycerol (Fig. 3 *C*).

To further understand the implication of the breakdown of hemextin AB complex in glycerol, we monitored its anticoagulant activity and that of the individual hemextins in buffers containing different concentrations of glycerol. The anticoagulant activity of hemextin AB complex decreased with the increase in glycerol concentration (Fig. 8 *B*). At 125 mM glycerol concentration there is no decrease in the anticoagulant activity. However, at 250 mM glycerol concentration (at which hemextin AB complex exists as a mixture of dimer and monomers; Fig. 7 *C*) there is a decrease in the anticoagulant activity. But this activity is higher than that of the anticoagulant effect of hemextin A alone. Therefore, we conclude that the dimer observed at 250 mM glycerol concentration exhibits the anticoagulant activity higher than hemextin A alone but lower than that of the tetramer. In other words, dimer formed in the presence of glycerol is different from the dimer formed in salt; the former dimer exhibiting an increased anticoagulant activity compared to hemextin A alone, whereas the latter not doing so. Glycerol, however, did not affect the anticoagulant activity of individual hemextins (Fig. 8 *B*).

The dissociation of the tetramer into dimer and monomers in the presence of glycerol indicates the importance of hydrophobic interactions in the tetrameric complex formation. This role of hydrophic interaction is further supported by the negative ΔC_p change observed during the formation of hemextin AB complex.

Our data strongly suggest that both electrostatic and hydrophobic interactions are important for the formation of tetrameric hemextin AB complex. To confirm that decrease in binding affinity between the monomers observed in salt and glycerol is not a solute osmotic effect, the K_A recorded in salt and glycerol was plotted against osmotic pressure (see Supplementary Material, Fig. S3). At similar osmolality of salt and glycerol decrease in binding affinity was more pronounced in salt than glycerol. This indicates that fall binding affinity is due to disruption of either electrostatic (for salt) or hydrophobic (for glycerol) interactions.

The effect of buffer conditions on the conformation of hemextins

Earlier studies using SEC (Fig. 7 *B*) and DLS (Fig. 3) indicated that hemextin A undergoes conformational changes in the presence of salt. We conducted 1D-NMR analysis to study the conformation of hemextins A and B under different buffer conditions (Fig. 9). In the presence of NaCl, there is a decrease in the number of Hα resonance peaks between 4.8 and 6 ppm in the case of hemextin A (Fig. 9 *A*). These chemical shifts contribute to the interresidue NOE crosspeaks between Hα of different amino acid residues forming antiparallel β-sheet structure typically observed in all three-finger toxins (57). Thus a decrease in the β-sheet content of hemextin A is observed in the presence of NaCl. In addition, there are several changes in the chemical shifts of side chains. A notable change is a highly shielded methyl peak that appears at the negative chemical shift value (-0.38 ppm) in the presence of salt. These observations strongly support conformational changes in hemextin A in the presence of NaCl. The overall dispersion of 1D proton NMR spectra of hemextin A in the

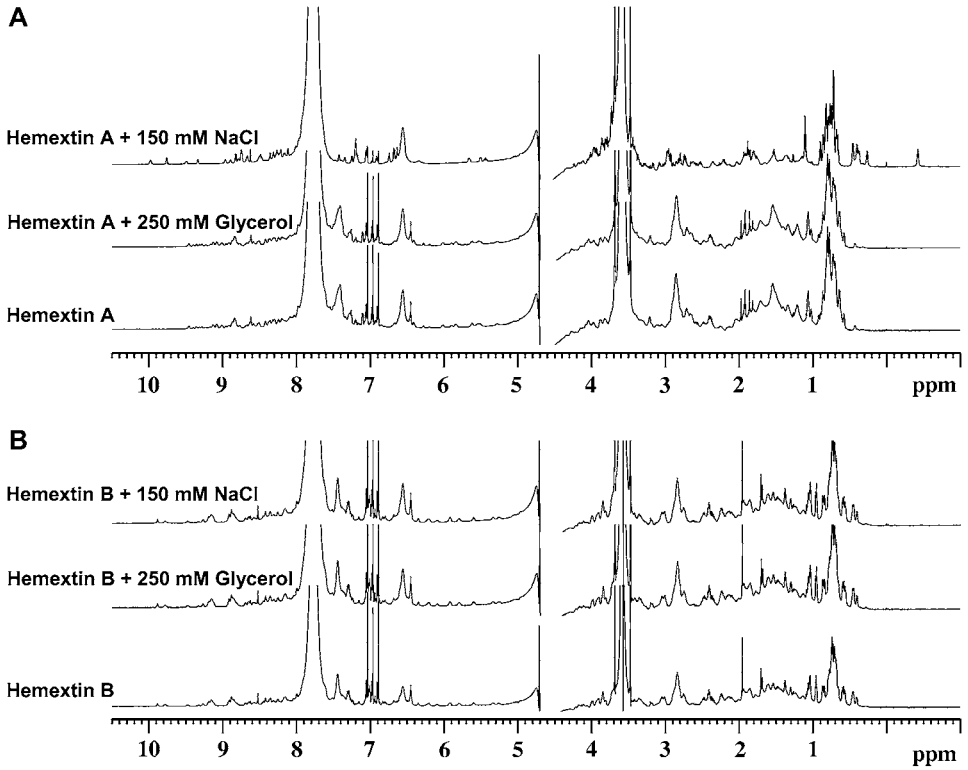

FIGURE 9 One-dimensional ^{1}H NMR studies. Spectrum of (*A*) hemextin A and hemextin B under different buffer conditions. Note that in the presence of salt, hemextin A undergoes a conformational change; also, the peaks are sharp throughout the spectrum. In addition, all 1D ^{1}H NMR spectra also exhibited a wide range of chemical shift dispersions (amide region 7–10 ppm, Hα region 3.8–6 ppm, and methyl region −0.4 –to 1.5 ppm), which is a characteristic of well-folded proteins. Therefore, the observed structural change is not due to resonance broadening or aggregation (because no aggregation state was observed as mentioned) but it is only due to addition of NaCl to hemextin A.

presence of glycerol (deuterated) remains the same with the subtle changes in the amide region (Fig. 9 *A*). Thus, hemextin A did not undergo any significant conformational change upon the addition of glycerol. Similar studies with hemextin B show that it did not undergo any significant conformational changes in the presence of NaCl or glycerol (Fig. 9 *B*) since there is almost one to one match for the spectral frequencies.

Model for hemextin AB complex

Based on our studies we propose a model for the assembly of hemextin AB complex (Fig. 10). Two molecules each of hemextin A and B form the tetrameric complex in Tris-HCl buffer (Fig. 10 *A*). The formation of this compact, synergistic complex is important for its anticoagulant activity. As illustrated earlier, hemextin AB dimer in high salt is different from the dimer formed in the presence of glycerol (Fig. 10 *C*). The former dimer has an apparent molecular diameter of 12.4 nm and lacks anticoagulant activity, whereas the latter has an apparent molecular diameter of 12.8 nm and exhibits slightly higher anticoagulant effects (Fig. 10 *C*). Thus, the breakdown of tetramer to dimer probably occurs in two different interfaces of interaction between hemextin A and B. One interface is sensitive to the ionic strength of its surroundings whereas the other is sensitive to glycerol (Fig. 10 *C*). Further, in the presence of salt, hemextin A undergoes conformational changes (Fig. 10 *B*) which may interfere in the tetramer formation. The dimer formed under high ionic conditions lacks the complete synergistic anticoagulant site (marked by a *dotted semicircle* in Fig. 10 *C*) and hence the resultant dimer is as active as hemextin A alone. (Fig. 8). In contrast, hydrophobic interactions are predominant in the second interface. Therefore, glycerol dissociates the tetramer into dimers. However, in this case only minor changes occur in the synergistic anticoagulant site of the complex (as shown in Fig. 10 *C*) and hence the resultant dimer is active (Fig. 8). We propose that the tetramer formation most likely stabilizes the anticoagulant site of hemextin A. The binding between hemextin AB complex/hemextin A and FVIIa has been characterized to validate the proposed model (Y. Banerjee, J. Mizuguchi, E. Person, R. Doley, S. Iwanaga, and R. Manjunatha Kini, unpublished data).

CONCLUSION

Hemextin AB complex is the first synergistic anticoagulant complex isolated from snake venom comprising solely two three-finger toxins—hemextin A and hemextin B (24). The tetrameric complex formation is a prerequisite for the synergistic inhibition of FVIIa. This complex formation is an enthalpically driven process. The complex exhibits identical apparent molecular diameters in gas and solution phases. Thermodynamics of hemextin AB complex formation indicates the absence of large-scale coupled folding. Both electrostatic and hydrophobic interactions are important for the assembly

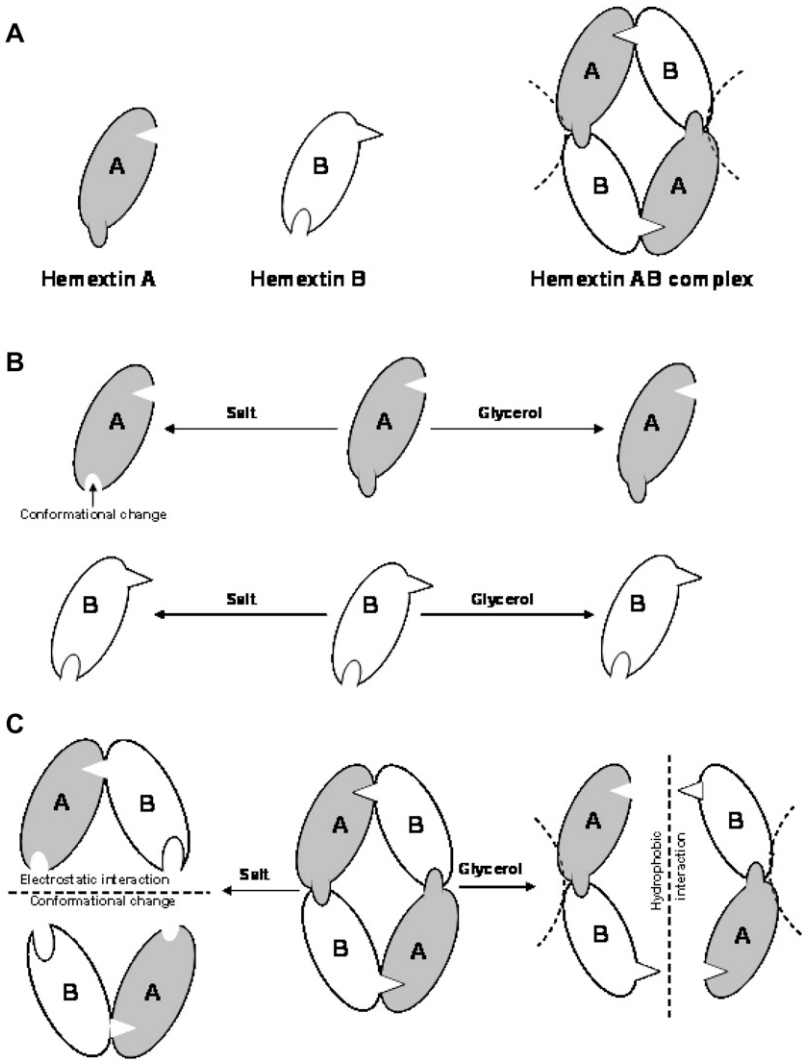

FIGURE 10 A proposed model of hemextin AB complex. (*A*) Schematic diagram depicting the formation of hemextin AB complex. Hemextins A and B, two structurally similar three-finger toxins, form a compact and rigid tetrameric complex with 1:1 stoichiometry (24). (*B*) Schematic diagram showing the effect of salt and glycerol on conformations of hemextins A and B. Hemextin A undergoes a conformational change in the presence of salt. (*C*) Dissociation of the tetrameric hemextin AB complex in the presence of salt and glycerol. The dissociation probably occurs in two different planes. Thus the hemextin AB dimer in high salt is different from the dimer formed in the presence of glycerol. Two putative anticoagulant sites are shown with dotted semicircles (see text for details).

of the tetramer. Based on our results we propose that the tetramer formation takes place by the participation of two interfaces. One of the interfaces is predominantly sensitive to the buffer ionic strength, indicating that electrostatic interactions are predominantly active in that interface. The other being sensitive to glycerol concentration of the solution indicates the participation of mostly hydrophobic interactions. The proposed model may help in a better understanding of the structure-function relationship of this novel anticoagulant complex.

SUPPLEMENTARY MATERIAL

To view all of the supplemental files associated with this article, visit www.biophysj.org.

We thank Dr. Jörg Rösgen (University of Texas Medical Branch) and Dr. Nina Sidorova and Dr. Donald Rau (National Institutes of Health/National Institute of Child Health & Human Development/Laboratory of Physical and Structural Biology) for kindly providing us the osmolality conversion tables and also for helpful discussions, Dr. Prakash Kumar (Department of Biological Sciences, National University of Singapore) for his constructive comments and for making the manuscript more succinct and concise, Dr. Peter Kuhn, Dr. Jeremiah Joseph, Dr. Subramanian Yegneswaran (The Scripps Research Institute), and Dr. Thomas Record Jr. (University of Wisconsin-Madison) for the helpful discussion. We also thank Gayathri Subramanian (Department of Chemistry, National University of Singapore) for her help in the DLS studies. Y.B. thanks the National University of Singapore for his research scholarship.

This work was supported in part by the Biomedical Research Council, Agency for Science and Technology, Singapore. The costs of publication of this article were defrayed in part by the payment of page charges. This article must therefore be hereby marked ''advertisement'' in accordance with 18 U.S.C. Section 1734 solely to indicate this fact.

REFERENCES

1. Davie, E. W., K. Fujikawa, and W. Kisiel. 1991. The coagulation cascade: initiation, maintenance, and regulation. *Biochemistry*. 30:10363–10370.

2. Davie, E. W. 1995. Biochemical and molecular aspects of the coagulation cascade. *Thromb. Haemost.* 74:1–6.
3. Nemerson, Y. 1988. Tissue factor and hemostasis. *Blood.* 71:1–8.
4. Yegneswaran, S., R. M. Mesters, and J. H. Griffin. 2003. Identification of distinct sequences in human blood coagulation factor Xa and prothrombin essential for substrate and cofactor recognition in the prothrombinase complex. *J. Biol. Chem.* 278:33312–33318.
5. Kumar, R., S. Beguin, and H. C. Hemker. 1995. The effect of fibrin clots and clot-bound thrombin on the development of platelet procoagulant activity. *Thromb. Haemost.* 74:962–968.
6. Myles, T., T. H. Yun, S. W. Hall, and L. L. Leung. 2001. An extensive interaction interface between thrombin and factor V is required for factor V activation. *J. Biol. Chem.* 276:25143–25149.
7. Saenko, E. L., D. Scandella, A. V. Yakhyaev, and N. J. Greco. 1998. Activation of factor VIII by thrombin increases its affinity for binding to synthetic phospholipid membranes and activated platelets. *J. Biol. Chem.* 273:27918–27926.
8. Curtis, J. E., S. L. Helgerson, E. T. Parker, and P. Lollar. 1994. Isolation and characterization of thrombin-activated human factor VIII. *J. Biol. Chem.* 269:6246–6251.
9. Mann, K. G., S. Butenas, and K. Brummel. 2003. The dynamics of thrombin formation. *Arterioscler. Thromb. Vasc. Biol.* 23:17–25.
10. Higgins, D. L., S. D. Lewis, and J. A. Shafer. 1983. Steady state kinetic parameters for the thrombin-catalyzed conversion of human fibrinogen to fibrin. *J. Biol. Chem.* 258:9276–9282.
11. Lewis, S. D., L. Lorand, J. W. Fenton, and J. A. Shafer. 1987. Catalytic competence of human alpha- and gamma-thrombin in the activation of fibrinogen and factor XIII. *Biochemistry.* 26:7597–7603.
12. Hanessian, S., R. Margarita, A. Hall, S. Johnstone, M. Tremblay, and L. Parlanti. 2002. Total synthesis and structural confirmation of the marine natural product Dysinosin A: a novel inhibitor of thrombin and Factor VIIa. *J. Am. Chem. Soc.* 124:13342–13343.
13. Carroll, A. R., G. K. Pierens, G. Fechner, L. P. De Almeida, A. Ngo, M. Simpson, E. Hyde, J. N. Hooper, S. L. Bostrom, D. Musil, and R. J. Quinn. 2002. Dysinosin A: a novel inhibitor of Factor VIIa and thrombin from a new genus and species of Australian sponge of the family Dysideidae. *J. Am. Chem. Soc.* 124:13340–13341.
14. Lindhout, T., J. Franssen, and G. Willems. 1995. Kinetics of the inhibition of tissue factor-factor VIIa by tissue factor pathway inhibitor. *Thromb. Haemost.* 74:910–915.
15. Salemink, I., J. Franssen, G. M. Willems, H. C. Hemker, and T. Lindhout. 1999. Inhibition of tissue factor-factor VIIa-catalyzed factor X activation by factor Xa-tissue factor pathway inhibitor. A rotating disc study on the effect of phospholipid membrane composition. *J. Biol. Chem.* 274:28225–28232.
16. Moons, A. H., R. J. Peters, N. R. Bijsterveld, J. J. Piek, M. H. Prins, G. P. Vlasuk, W. E. Rote, and H. R. Buller. 2003. Recombinant nematode anticoagulant protein c2, an inhibitor of the tissue factor/factor VIIa complex, in patients undergoing elective coronary angioplasty. *J. Am. Coll. Cardiol.* 41:2147–2153.
17. Lee, A. Y., and G. P. Vlasuk. 2003. Recombinant nematode anticoagulant protein c2 and other inhibitors targeting blood coagulation factor VIIa/tissue factor. *J. Intern. Med.* 254:313–321.
18. Baugh, R. J., G. J. Broze, Jr., and S. Krishnaswamy. 1998. Regulation of extrinsic pathway factor Xa formation by tissue factor pathway inhibitor. *J. Biol. Chem.* 273:4378–4386.
19. Broze, G. J. Jr., and J. P. Miletich. 1987. Characterization of the inhibition of tissue factor in serum. *Blood.* 69:150–155.
20. Sanders, N. L., S. P. Bajaj, A. Zivelin, and S. I. Rapaport. 1985. Inhibition of tissue factor/factor VIIa activity in plasma requires factor X and an additional plasma component. *Blood.* 66:204–212.
21. Buddai, S. K., L. Toulokhonova, P. W. Bergum, G. P. Vlasuk, and S. Krishnaswamy. 2002. Nematode anticoagulant protein c2 reveals a site on factor Xa that is important for macromolecular substrate binding to human prothrombinase. *J. Biol. Chem.* 277:26689–26698.
22. Kini, R. M. 2006. Anticoagulant proteins from snake venoms: structure, function and mechanism. *Biochem. J.* 397:377–387.
23. Kini, R. M. 2005. Serine proteases affecting blood coagulation and fibrinolysis from snake venoms. *Pathophysiol. Haemost. Thromb.* 34: 200–204.
24. Banerjee, Y., J. Mizuguchi, S. Iwanaga, and R. M. Kini. 2005. Hemextin AB complex, a unique anticoagulant protein complex from *Hemachatus haemachatus* (African Ringhals cobra) venom that inhibits clot initiation and factor VIIa activity. *J. Biol. Chem.* 280:42601–42611.
25. Banerjee, Y., J. Mizuguchi, S. Iwanaga, and R. M. Kini. 2005. Hemextin AB complex—a snake venom anticoagulant protein complex that inhibits factor VIIa activity. *Pathophysiol. Haemost. Thromb.* 34:184–187.
26. Wang, R., R. M. Kini, and M. C. Chung. 1999. Rhodocetin, a novel platelet aggregation inhibitor from the venom of *Calloselasma rhodostoma* (Malayan pit viper): synergistic and noncovalent interaction between its subunits. *Biochemistry.* 38:7584–7593.
27. Paaventhan, P., C. Kong, J. S. Joseph, M. C. Chung, and P. R. Kolatkar. 2005. Structure of rhodocetin reveals noncovalently bound heterodimer interface. *Protein Sci.* 14:169–175.
28. Rao, V. S., and R. M. Kini. 2002. Pseutarin C, a prothrombin activator from *Pseudonaja textilis* venom: its structural and functional similarity to mammalian coagulation factor Xa-Va complex. *Thromb. Haemost.* 88:611–619.
29. Rao, V. S., S. Swarup, and R. M. Kini. 2003. The nonenzymatic subunit of pseutarin C, a prothrombin activator from eastern brown snake (*Pseudonaja textilis*) venom, shows structural similarity to mammalian coagulation factor V. *Blood.* 102:1347–1354.
30. Knutson, E. O., and K. T. Whitby. 1975. Aerosol classification by electric mobility: apparatus, theory, and applications. *J. Aerosol Sci.* 6:443–451.
31. Provencher, S. W. 1976. A Fourier method for the analysis of exponential decay curves. *Biophys. J.* 16:27–41.
32. Levenberg, K. 1944. A method for the solution of certain problems in least squares. *Q. Appl. Math.* 2:164–168.
33. Marquardt, D. 1963. An algorithm for least-squares estimation of nonlinear parameters. *SIAM J. Appl. Math.* 11:431–441.
34. Lakshminarayanan, R., E. O. Chi-Jin, X. J. Loh, R. M. Kini, and S. Valiyaveettil. 2005. Purification and characterization of a vaterite-inducing peptide, pelovaterin, from the eggshells of *Pelodiscus sinensis* (Chinese soft-shelled turtle). *Biomacromolecules.* 6:1429–1437.
35. Piotto, M., V. Saudek, and V. Sklenar. 1992. Gradient-tailored excitation for single-quantum NMR spectroscopy of aqueous solutions. *J. Biomol. NMR.* 2:661–665.
36. Wilkins, D. K., S. B. Grimshaw, V. Receveur, C. M. Dobson, J. A. Jones, and L. J. Smith. 1999. Hydrodynamic radii of native and denatured proteins measured by pulse field gradient NMR techniques. *Biochemistry.* 38:16424–16431.
37. Lu, H., B. Isralewitz, A. Krammer, V. Vogel, and K. Schulten. 1998. Unfolding of titin immunoglobulin domains by steered molecular dynamics simulation. *Biophys. J.* 75:662–671.
38. Longhi, S., V. Receveur-Brechot, D. Karlin, K. Johansson, H. Darbon, D. Bhella, R. Yeo, S. Finet, and B. Canard. 2003. The C-terminal domain of the measles virus nucleoprotein is intrinsically disordered and folds upon binding to the C-terminal moiety of the phosphoprotein. *J. Biol. Chem.* 278:18638–18648.
39. Perozzo, R., G. Folkers, and L. Scapozza. 2004. Thermodynamics of protein-ligand interactions: history, presence, and future aspects. *J. Recept. Signal Transduct. Res.* 24:1–52.
40. Velazquez-Campoy, A., S. A. Leavitt, and E. Freire. 2004. Characterization of protein-protein interactions by isothermal titration calorimetry. *Methods Mol. Biol.* 261:35–54.
41. Weber, P. C., and F. R. Salemme. 2003. Applications of calorimetric methods to drug discovery and the study of protein interactions. *Curr. Opin. Struct. Biol.* 13:115–121.
42. Katragadda, M., D. Morikis, and J. D. Lambris. 2004. Thermodynamic studies on the interaction of the third complement component and its inhibitor, compstatin. *J. Biol. Chem.* 279:54987–54995.

43. Tidor, B., and M. Karplus. 1994. The contribution of vibrational entropy to molecular association. The dimerization of insulin. *J. Mol. Biol.* 238:405–414.

44. Stites, W. E. 1997. Protein-protein interactions: interface structure, binding thermodynamics, and mutational analysis. *Chem. Rev.* 97: 1233–1250.

45. Murphy, K. P., and S. J. Gill. 1991. Solid model compounds and the thermodynamics of protein unfolding. *J. Mol. Biol.* 222:699–709.

46. Murphy, K. P., and E. Freire. 1992. Thermodynamics of structural stability and cooperative folding behavior in proteins. *Adv. Protein Chem.* 43:313–361.

47. Cooper, A. 1999. Thermodynamic analysis of biomolecular interactions. *Curr. Opin. Chem. Biol.* 3:557–563.

48. Dunitz, J. D. 1995. Win some, lose some: enthalpy-entropy compensation in weak intermolecular interactions. *Chem. Biol.* 2:709–712.

49. Lumry, R. 2003. Uses of enthalpy-entropy compensation in protein research. *Biophys. Chem.* 105:545–557.

50. Spolar, R. S., and M. T. Record, Jr. 1994. Coupling of local folding to site-specific binding of proteins to DNA. *Science.* 263:777–784.

51. von Hippel, P. H. 1994. Protein-DNA recognition: new perspectives and underlying themes. *Science.* 263:769–770.

52. Finkelstein, A. V., and J. Janin. 1989. The price of lost freedom: entropy of bimolecular complex formation. *Protein Eng.* 3:1–3.

53. Janin, J., and C. Chothia. 1978. Role of hydrophobicity in the binding of coenzymes. Appendix. Translational and rotational contribution to the free energy of dissociation. *Biochemistry.* 17:2943–2948.

54. Hilpert, K., H. Wessner, J. Schneider-Mergener, K. Welfle, R. Misselwitz, H. Welfle, A. C. Hocke, S. Hippenstiel, and W. Hohne. 2003. Design and characterization of a hybrid miniprotein that specifically inhibits porcine pancreatic elastase. *J. Biol. Chem.* 278:24986–24993.

55. Liu, W., D. Bratko, J. M. Prausnitz, and H. W. Blanch. 2004. Effect of alcohols on aqueous lysozyme-lysozyme interactions from static light-scattering measurements. *Biophys. Chem.* 107:289–298.

56. Livingstone, J. R., R. S. Spolar, and M. T. Record, Jr. 1991. Contribution to the thermodynamics of protein folding from the reduction in water-accessible nonpolar surface area. *Biochemistry.* 30:4237–4244.

57. Kini, R. M. 2002. Molecular moulds with multiple missions: functional sites in three-finger toxins. *Clin. Exp. Pharmacol. Physiol.* 29:815–822.